JOURNAL OF

SEISMIC EXPLORATION

Volume 20, Number 1 February 2011

CONTENTS

JOURNAL OF SEISMIC EXPLORATION

Volume 20, Number 1, February 2011

Indexed/Abstracted in: Current Contents, Petroleum Abstracts, Geo Abstracts, GEOBASE, SciSearch and Research Alert.

ISSN 0963 - 0651

Printed by RG Productions, London

JOURNAL OF

SEISMIC EXPLORATION

Volume 20, 2011

GEOPHYSICAL PRESS

THE DIRECT-ARRIVAL-REMOVAL METHOD OF WAVEFORM INVERSION IN THE LAPLACE DOMAIN FOR A DEEP-WATER MODEL

DONGKWEON LEE and CHANGSOO SHIN

Department of Energy Systems Engineering, Seoul National University, 599 Gwanak-ro, Gwanak-gu, Seoul 151-742, South Korea.

(Received January 8, 2010; revised version accepted October 1, 2010)

ABSTRACT

Lee, D. and Shin, C.S., 2011. The direct-arrival-removal method of waveform inversion in the Laplace domain for a deep-water model. *Journal of Seismic Exploration*, 20: 1-22.

Waveform inversion has achieved advances in both the time and frequency domains. However, the process still has difficulties when applied to survey data because of the absence of low-frequency components. Recently, the development of waveform inversion in the Laplace domain has resulted in the stable convergence of field data using the Laplace-transformed wavefields. Because the early-arrival wavefield is more sensitive when taking the Laplace-transformed wavefield, the mismatches in the direct-arrival wavelets resulting from the Lloyd mirror effect and the noise in the early wavefield cause large errors in the Laplace waveform inversion.

In this study, we developed a direct-arrival-removal method (DARM) to implement waveform inversion on field data obtained in a deep-water environment. We also introduced a new objective function and a source-estimation method using the DARM.

In order to validate DARM method for waveform inversion in Laplace domain, we compared DARM with a conventional waveform inversion in the Laplace domain for a synthetic model. When we applied both DARM and conventional Laplace waveform inversion to derive the velocity structure from field data which is acquired from deep-water, the result from DARM shows more accurate than that of conventional method.

KEY WORDS: waveform inversion, Laplace, objective function, source estimation, deep water, direct arrival.

0963-0651/11/$5.00

INTRODUCTION

In the 1980's, waveform inversion using prestack seismic data was developed. Tarantola (1984) implemented waveform inversion using a gradient-direction method with prestack seismic-survey data in the time domain. He calculated the gradients using a back-propagating method which, for computational efficiency, did not directly calculate the partial derivatives. Pratt (1998) developed a waveform inversion in the frequency domain by a similar method to that used for the time domain. The waveform inversion was applied to other fields such as seismic refraction surveying (Min and Shin, 2006).

However, conventional waveform inversion had a limitation on the initial velocity model. If the initial model was not close to the actual conditions, a meaningful solution could not be obtained. Therefore, to overcome this limitation in the waveform inversion, several techniques were utilized to invert from the low-frequency band to a wide-frequency band (Kim et al., 2009). However, it was not easily applied to field data where there was no confidence in the representation of the low frequency field.

Shin and Cha (2008) developed a waveform inversion using Laplace-transformed wavelets which had advantages for inverting a velocity structure with a long wavelength in the spatial wavenumber domain. Laplace waveform inversion was able to find an anomalous velocity from the background velocity which was varied gradually from low to high. Additionally, the waveform inversion in the Laplace domain had a smaller possibility of falling into local minima from an improper starting model than the waveform inversions in the other domains (Shin and Ha, 2008). This result from waveform inversion in the Laplace domain could be applied to prestack depth migration for a given-velocity model or a waveform inversion in the frequency domain as an initial-velocity model where the velocity model from the Laplace waveform inversion has a long spatial wavelength. However, waveform inversion in the Laplace domain still has limitations in deep-water environments. In the inversion of field data obtained in the deep-water environment, it is difficult to reduce the residuals in direct waves by modeling using the finite-element method (FEM) because of both the Lloyd mirror effect and the complex radiation features. Also, as the radiated energy is rapidly reduced to below the background noise level along the offset, early noise makes the Laplace transformation unstable.

In this study, a direct-arrival-removal method (DARM) was developed for waveform inversion in the Laplace domain. It implies the algorithm for a new objective function and source-estimation method. We applied DARM to a synthetic model and compared this with a waveform inversion using the conventional logarithmic norm method. Finally, we applied the algorithm to field data, and the reconstructed velocity structure was employed in the reverse time migration.

DEEP-WATER DATA

Fig. 1(a) shows one of the commonly used shot gathers in deep-water environments. The distance between the airgun array and the first hydrophone group is 172 m, the gap in the two hydrophone groups is 25 m, and the number of receivers is 320. The reflection wave from the sea floor in near offset is recorded about 2.5 seconds later because the water depth is greater than 1.8 km. In this common shot gather, the noise before the first direct arrival can be seen. This noise causes a critical error in transforming the wavelets into the Laplace domain; thus it is necessary to eliminate this noise. Various methods are available for eliminating this early noise.

Fig. 1(b) shows the shot gather with muting applied to the noise before the direct-arrival wave in near offset, as well as the noise itself, including the direct-arrival wave where the magnitude of the direct-arrival wave is less than that of the noise. To perform the Laplace waveform inversion, it is necessary to mute the early noise (Shin and Cha, 2008). While there is another method to mute the noise, i.e., to regard it as a constant velocity (which is 1.5 km/s as a rule of thumb), the former is superior to the latter.

Fig. 1(c) shows the shot gather with muting applied to all signals above the first reflection from the bottom. The direct-arrival wave propagated horizontally from the airgun does not contain subsurface information. Thus, it is certain that eliminating the most noise, including the direct-arrival wave, is proper for the implementation of the inversion in the Laplace domain. In the case of the early arrival time of the reflection wave from a shallow sea or land

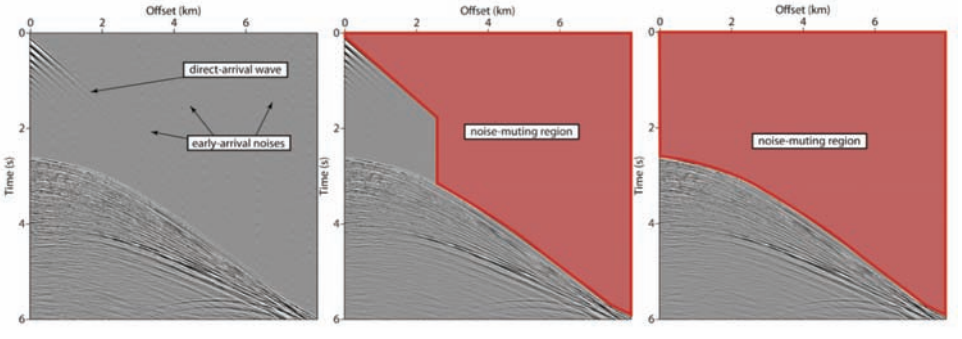

(a) (b) (c)

Fig. 1. (a) Shot gather shows data obtained from a deep-water field. (b) To implement the Laplace waveform inversion, the noise above a distinguishable direct-arrival wave was muted. (c) The noise and direct-arrival wave were both muted.

data, this DARM seems difficult to apply, but in the case of a deep-water survey, the Laplace waveform inversion using DARM can be more stable and more robust. This is because the removal of the direct-arrival wave means the elimination of both the direct wave, which does not contain subsurface information, and the early noise, which makes the Laplace-transformed wavelet unstable.

Fig. 2(a) shows the Laplace-transformed wavelet of Fig. 1(b). The vertical axis has a logarithmic scale, and the horizontal axis indicates the distance. The early wavefield has a much larger value than the late-arrival signal by Laplace transform. Thus, the noise contaminated the Laplace wavefield. Additionally, we can see the discontinuous distribution of the wavefield at the interface in the case where noise below the level of the direct-arrival wave is muted.

Fig. 2(b) shows the Laplace-transformed wavelet of Fig. 1(c). Unlike in Fig. 2(a), here we can see a continuous distribution of the wavefield.

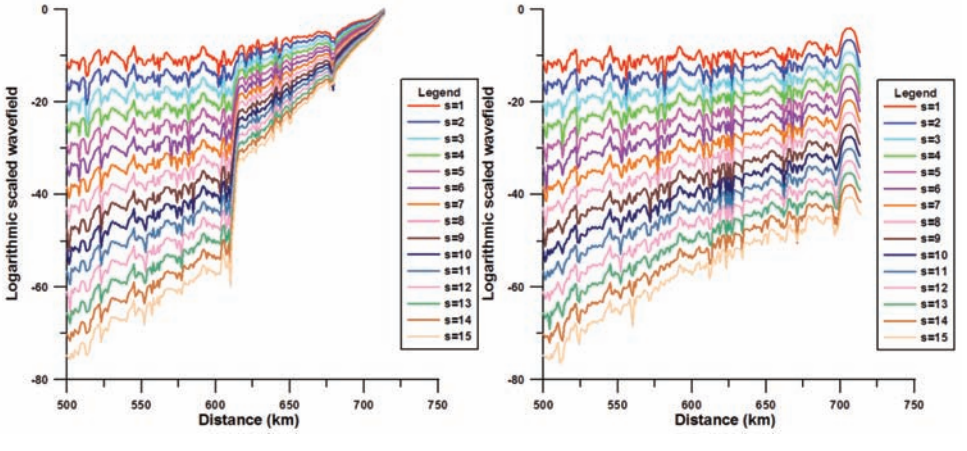

Fig. 2. (a) The Laplace-transformed wavefields from Fig. 1(b). (b) The Laplace-transformed wavefields from Fig. 1(c).

THEORY

The waveform inversion in the Laplace domain

The finite-element formulation of the wave equation in the time domain is given by:

$$\mathbf{M}\ddot{\mathbf{u}} + \mathbf{C}\dot{\mathbf{u}} + \mathbf{K}\mathbf{u} = \mathbf{f} \quad , \tag{1}$$

where $\mathbf{M}$ is the mass matrix, $\mathbf{C}$ is the damping matrix, $\mathbf{K}$ is the stiffness matrix, $\mathbf{u}$ is a wavefield in the time domain, and $\mathbf{f}$ is a source vector. The wave equation in the Laplace domain is as follows (Shin and Cha, 2008):

$$\mathbf{S}\tilde{\mathbf{u}} = \tilde{\mathbf{f}} \quad , \tag{2}$$

where the impedance matrix is $\mathbf{S} = \mathbf{M}s^2 + \mathbf{C}s + \mathbf{K}$, and s is a Laplacian damping constant (Shin and Cha, 2008). The wavefield in the Laplace domain is $\tilde{\mathbf{u}} = \int_0^\infty u(t)e^{-st}dt$, and the source vector is $\tilde{\mathbf{f}}$.

To implement the waveform inversion, the objective function is as follows:

$$E = \| J(\tilde{\mathbf{u}},s) \| \quad , \tag{3}$$

where J is a function of complex variables and $\| \cdot \|$ is a least-squares operator. Using a least-squares method, E is given by:

$$E = \tfrac{1}{2} \sum_j \delta r_j \overline{\delta r_j} \quad , \tag{4}$$

where δr_j is the mismatch between the modeling result and the observed data from the j-th receiver.

Minimizing E implies to find the gradient ∇E, or equivalently $\partial E/\partial p_m$, for every parameter p_m. Differentiating eq. (2) with respect to a model parameter p_m , we obtain:

$$(\partial \mathbf{S}/\partial p_m)\tilde{\mathbf{u}} + (\partial \tilde{\mathbf{u}}/\partial p_m)\mathbf{S} = 0 \quad , \quad m = 1,2,\ldots,n_m \tag{5}$$

$$\partial \tilde{\mathbf{u}}/\partial p_m = \mathbf{S}^{-1}\mathbf{v}_m \quad , \quad m = 1,2,\ldots,n_m \tag{6}$$

where $\mathbf{v}_m = -(\partial \mathbf{S}/\partial p_m)\tilde{\mathbf{u}}$, and then $\mathbf{v}_m$ is the virtual source vector. And the virtual source vector is back-propagated to obtain the partial derivative wavefields perturbed by the m-th model parameter p_m (Pratt et al., 1998).
Eq. (6) defines the partial derivative wavefield.

Objective function in the DARM

Here, $\tilde{\mathbf{d}}'$ is the observed wavefield of the direct-arrival muted data, and $\tilde{\mathbf{u}}'$ is the modeled wavefield of the directly removed data in the transformed domain. Using the direct-arrival-removed data, the residual of the recorded wavefield from the j-th receiver is:

$$\delta r_j = \ln \tilde{u}'_j - \ln \tilde{d}'_j = \ln(\tilde{u}'_j/\tilde{d}'_j) = \ln[(\tilde{u}_j - \tilde{h}_j)/\tilde{d}'_j] \quad , \tag{7}$$

where $\tilde{u}_j$ is the modeled wavefield of the j-th receiver for the given velocity and $\tilde{h}_j$ is the direct-only wavefield of the same receiver. In the Laplace domain, as the receiver array moves farther away the amplitude of the transformed wavefield rapidly decreases. An objective function using a log-transformed wavefield is superior to a conventional objective function using the L_2 norm (Shin and Cha, 2008). Thus, the objective function of the DARM using a logarithmic wavefield is:

$$E = \tfrac{1}{2} \sum_j |\ln[(\tilde{u}_j - \tilde{h}_j)/\tilde{d}'_j]|^2 \quad . \tag{8}$$

If the inversion of the steepest-descent method is implemented, the gradient direction will be the dot product between the partial derivatives and residuals:

$$\partial E/\partial p_m = \mathrm{Re}\Big[\sum_j \{[1/(\tilde{u}_j - \tilde{h}_j)](\partial \tilde{u}_j/\partial p_m)\overline{\ln[(\tilde{u}_j - \tilde{h}_j)/\tilde{d}'_j]}\} \Big] \quad , \tag{9}$$

where p_m is a model parameter for a velocity property, $\partial E/\partial p_m$ is the steepest-descent direction of the m-th model parameter, and $\partial \tilde{u}_j/\partial p_m$ is the partial derivative of p_m. Transposing the partial-derivative wavefield, expressed in terms of the complex impedance matrix, $\mathbf{S}$, and the virtual source, $\mathbf{v}_m$, in eq.(6), and substituting it into eq. (9) yields:

$$\partial E/\partial p_m = \mathrm{Re}[(\mathbf{v}_m)^t \mathbf{S}^{-1} \hat{\mathbf{r}}] \quad , \tag{10}$$

where:

$$\hat{\mathbf{r}} = \begin{pmatrix} [1/(\tilde{u}_1 - \tilde{h}_1)](\partial \tilde{u}_1/\partial p_m)\overline{\ln[(\tilde{u}_1 - \tilde{h}_1)/\tilde{d}'_1]} \\ [1/(\tilde{u}_2 - \tilde{h}_2)](\partial \tilde{u}_2/\partial p_m)\overline{\ln[(\tilde{u}_2 - \tilde{h}_2)/\tilde{d}'_2]} \\ \vdots \\ [1/(\tilde{u}_{n_r} - \tilde{h}_{n_r})](\partial \tilde{u}_{n_r}/\partial p_m)\overline{\ln[(\tilde{u}_{n_r} - \tilde{h}_{n_r})/\tilde{d}'_{n_r}]} \end{pmatrix} \quad .$$

Eq. (10) was adapted using the back-propagation theory of reverse time migration (Shin and Min, 2006).

Source estimation

The wavefield recorded from the j-th receiver is described by following the amplitude and the phase of the wave signal (Shin et al., 2007):

$$\tilde{\mathbf{u}}_j = B_j C e^{i(\theta_{cal1,j}+\theta_{src})} \quad , \tag{11}$$

$$\tilde{\mathbf{u}}_{h,j} = B_{h,j} C e^{i(\theta_{cal2,j}+\theta_{src})} \quad , \tag{12}$$

where C is the amplitude and θ_{src} is the phase of the source wavelet; B_j and $\theta_{cal1,j}$ are the amplitude and phase, respectively, of the Green's function wavefield of a given-velocity model at the j-th receiver; and $B_{j,h}$ and $\theta_{cal2,j}$ are the amplitude and phase, respectively, of the Green's function wavefield of a homogeneous model. Therefore, a logarithmically scaled residual of the direct-removal wave field is as follows:

$$\begin{aligned} \delta r_j &= \ln[(B_j C e^{i(\theta_{cal1,j}+\theta_{src})} - B_{h,j} C e^{i(\theta_{cal2,j}+\theta_{src})})/A_j e^{i\theta_{obs,j}}] \\ &= \ln[(B_j e^{i(\theta_{cal1,j})} - B_{h,j} e^{i(\theta_{cal2,j})})/A_j e^{i\theta_{obs,j}}] C e^{\theta_{src}} \\ &= \ln C_g e^{\theta_g} C e^{\theta_{src}} \quad , \end{aligned} \tag{13}$$

where $C_g e^{\theta_g}$ is the residual calculated by the solution of the Green's function and the logarithmic scale z is $z = \ln C$.

By Newton's method, the source estimation is:

$$\delta p^k = -\mathbf{H}^{-1} \nabla_p E^k \quad , \tag{14}$$

where δp^k is the update parameter for the k-th iteration and $\mathbf{H}$ is the Hessian matrix.

The gradient direction of the objective function is then:

$$\nabla_{\theta_{src}} \mathbf{E} = \sum_j \delta\theta_j \quad , \tag{15}$$

$$\nabla_z \mathbf{E} = \sum_j (z + \ln C_g) \quad . \tag{16}$$

Therefore, for the amplitude and phase, the update parameters for each k-th iteration are, respectively:

$$\delta p_{\theta}^{k} = -[\sum_{j} \delta\theta_{j}]/[\sum_{j} 1] \quad , \tag{17}$$

and

$$\delta p_{Z}^{k} = -[\sum_{j} (z + \ln C_{g})]/[\sum_{j} 1] \quad . \tag{18}$$

INVERSION RESULTS

Synthetic inversion test: Laplace-domain finite-element modeling (BP model)

The BP model (Billette and Brandsberg-Dhal, 2005) has complex structures including a salt dome interpenetrating the background layered structure. Salt domes and subsalt structures are very interesting targets for inversion benchmarks. In order to construct a deep-water model, we modified the BP model by adding a 500-m water layer on top. And we used deep part of BP model which had 46 km distance along the horizontal axis. In this synthetic model test, the BP model was resampled into a 25 × 25 m grid size for both horizontal and vertical coordinates. Fig. 3 shows the new BP model modified for the deep-water test.

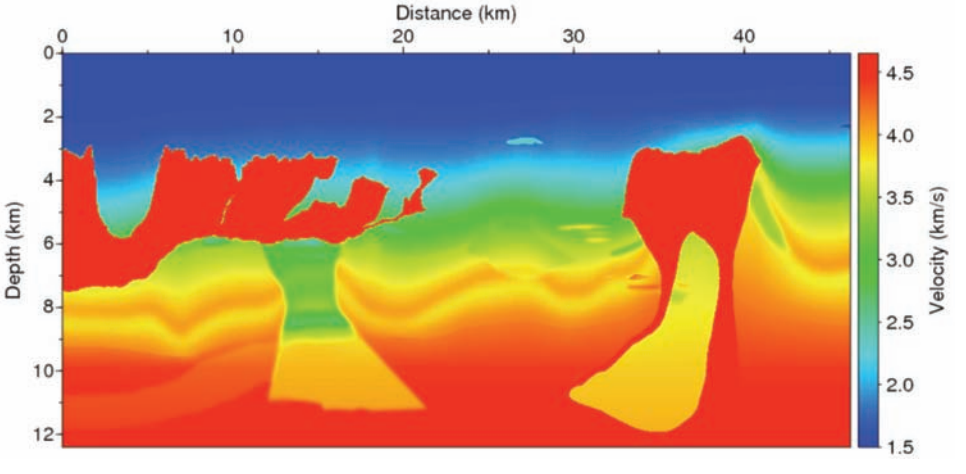

Fig. 3. The modified BP velocity model for a synthetic test that implies a deep-water condition. We resampled it to a 25 × 25 m grid size and added a 500-m water layer.

The Laplace damping constant for both modeling and inversion was used by s = 1,2,…,15. And the recorded time length was 12 s. The source signal was the first derivative of a Gaussian wavelet, and its maximum frequency was 18 Hz. The synthetic seismogram was generated in the Laplace domain, and the inversion was also implemented in the Laplace domain. Fig. 4 shows the wavefields from each Laplace damping constants, s. The vertical axis has a logarithmic scale to illustrate how the Laplace wavefield decays rapidly as distance increase. This decay also becomes more rapid as the Laplace damping constant was increased.

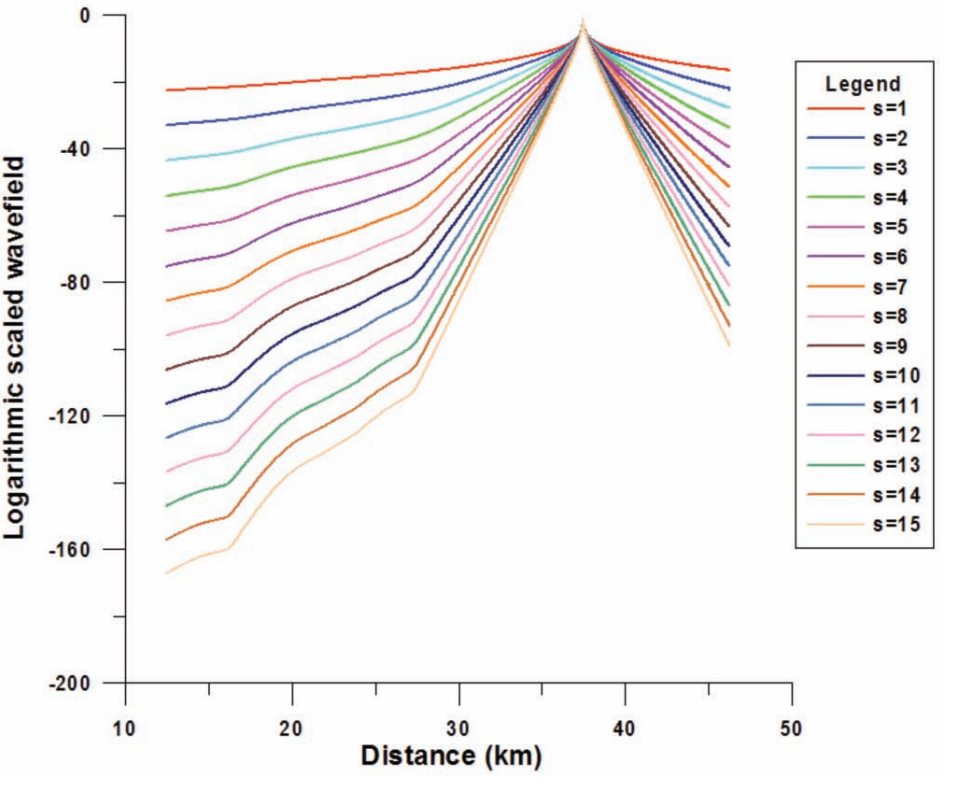

Fig. 4. The Laplace wavefields with logarithmic scales at 38 km distance from the source position.

Fig. 5(a) shows the initial-velocity model, which increases from 1.5 km/s to 4.5 km/s. Fig. 5(b) shows the velocity result, which is derived by the application of an objective function using a logarithmic wavefield (Shin and Cha, 2008); we term this the conventional Laplace waveform inversion. The waveform inversion in the Laplace domain well defines the top structure of the salt dome; the velocity gradient is more sensitive for the velocity variance of the subsurface and less sensitive for that at deeper positions.

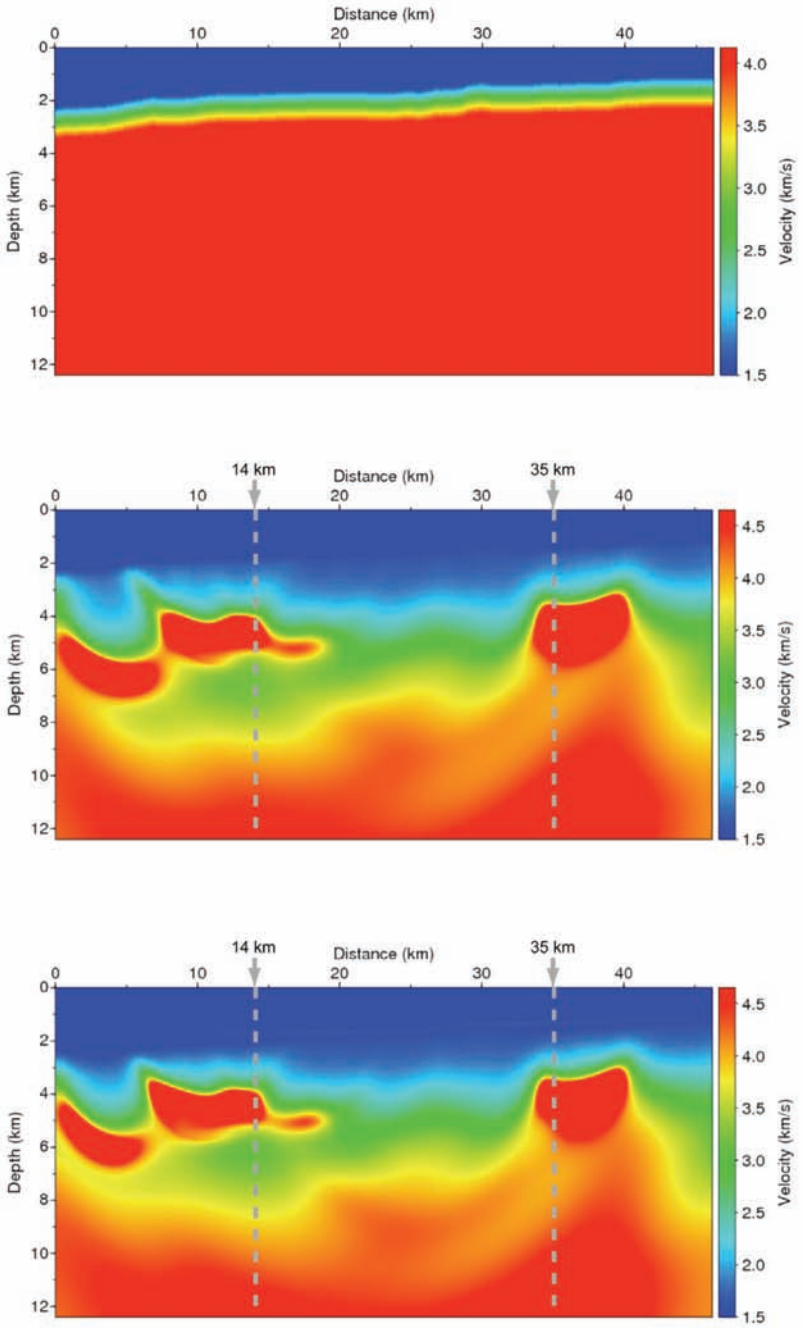

Fig. 5. (a) The initial-velocity model for the synthetic inversion test. (b) The result from a conventional waveform inversion in the Laplace domain. (c) The result of the DARM. The dotted lines are the positions for plotting the vertical velocity section.

The waveform inversion in the frequency domain provides a velocity result with high resolution but often fails to obtain the correct background velocity. Hence, the waveform inversion in the Laplace domain can provide a smooth background velocity (Shin and Cha, 2008). The waveform inversion in the Laplace domain offers only a long wave-number velocity model and as such is different from the waveform inversion in the frequency domain; but the velocity result is well matched in the sense of having a smooth structure, so it is also useful for the initial velocity for waveform inversion in the frequency domain or the migration velocity. Below a depth of 7 km, the inversion fails to find the true velocity. If the sea bottom is deep, the water layer in the upper zone of an inversion model needs a constraint for the velocity update. Fig. 5(c) shows the result of the DARM. Here, the velocity result is similar to that of the conventional waveform inversion in the Laplace domain.

To compare the inverted velocities with the true velocity, we chose two vertical velocity profiles. Fig. 6(a) shows the velocity profile at 14 km distance. The salt is at a depth of 3.5 km, and its velocity is 4.5 km/s. In this graph, both the DARM and the conventional method show similar inverted velocities. Fig. 6(b) shows the velocities at 35 km distance. Both methods show appropriate inversion results and obtained good velocity results in the sense of long wavelengths result.

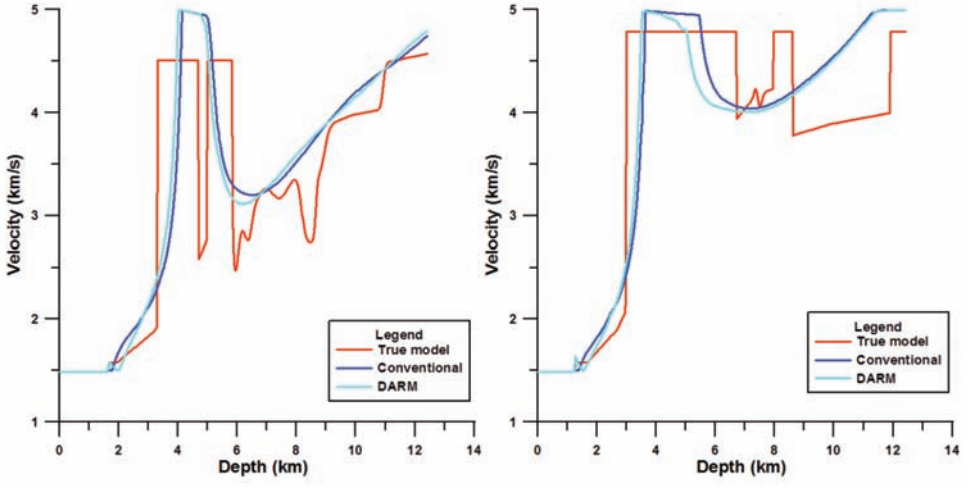

(a) (b)

Fig. 6. Velocity profiles: (a) at 14 km distance; (b) at 35 km distance.

In the synthetic test, we cannot find much difference between both methods. It is because the direct arrival wavelet has little contribution to obtaining the subsurface velocity. We are able to infer that we will obtain almost the same subsurface velocity of the conventional inversion using DARM.

Fig. 7 shows the source wavelet applied to the synthetic modeling that is to be transformed into the Laplace domain (solid line), the result from conventional source estimation that uses the full wavefield (diamond symbol), and the result from the DARM (triangle symbol), which applied the source-estimation algorithm using the direct-arrival-removal wavefield. For both inversions, we used the initial guess value by 1. In source estimation, the full Newton method yields an accurate source wavelet.

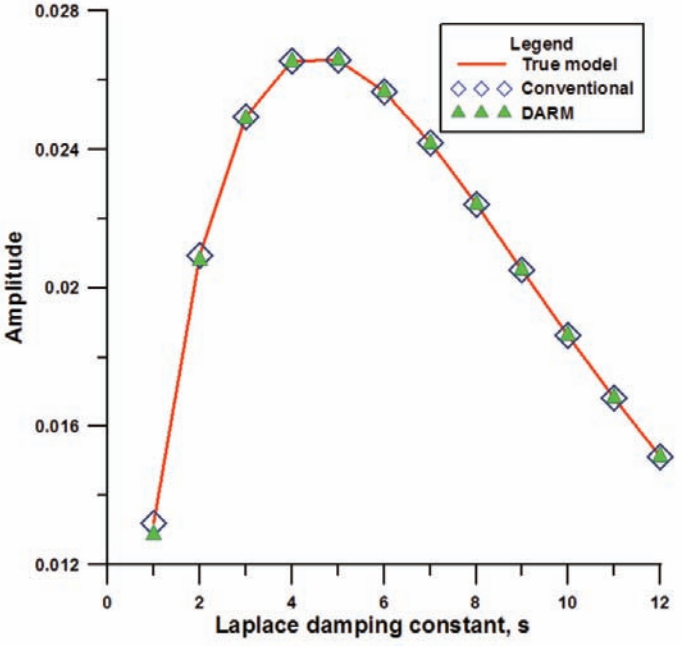

Fig. 7. Solid line: the source wavelet for the first derivative of the Gaussian wavelet in the Laplace domain: diamonds, source wavelet estimated by conventional waveform inversion in the Laplace domain; triangles, source wavelet estimated by DARM in the Laplace domain.

Synthetic inversion test: time-domain finite-difference modeling (Pluto model)

In this test, we created synthetic data using a time-domain FDM, which has fourth-order accuracy, and took a Laplace transform of the forward data. We used a Pluto model for the deep-water data. The Pluto model implies three large salt structures, and its background velocity increases smoothly.

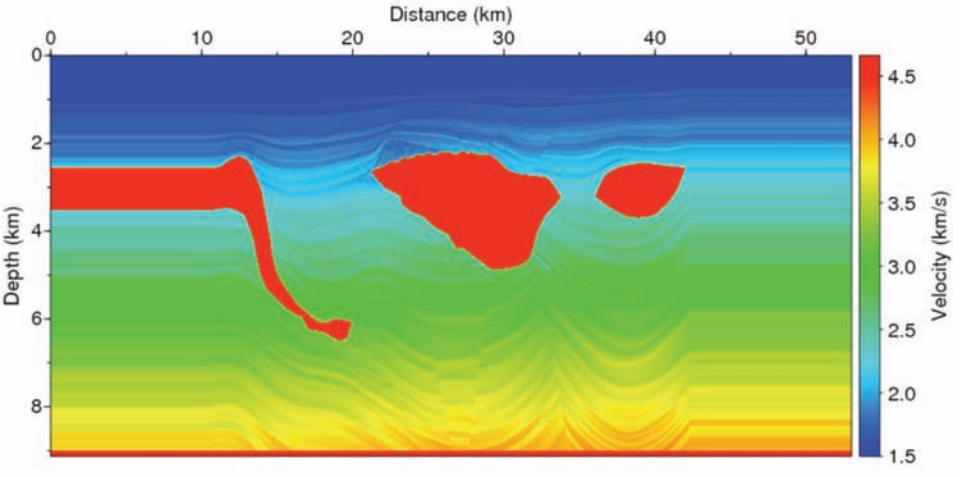

Fig. 8. The Pluto V_P model for the Laplace waveform inversion test from the time-domain modeling.

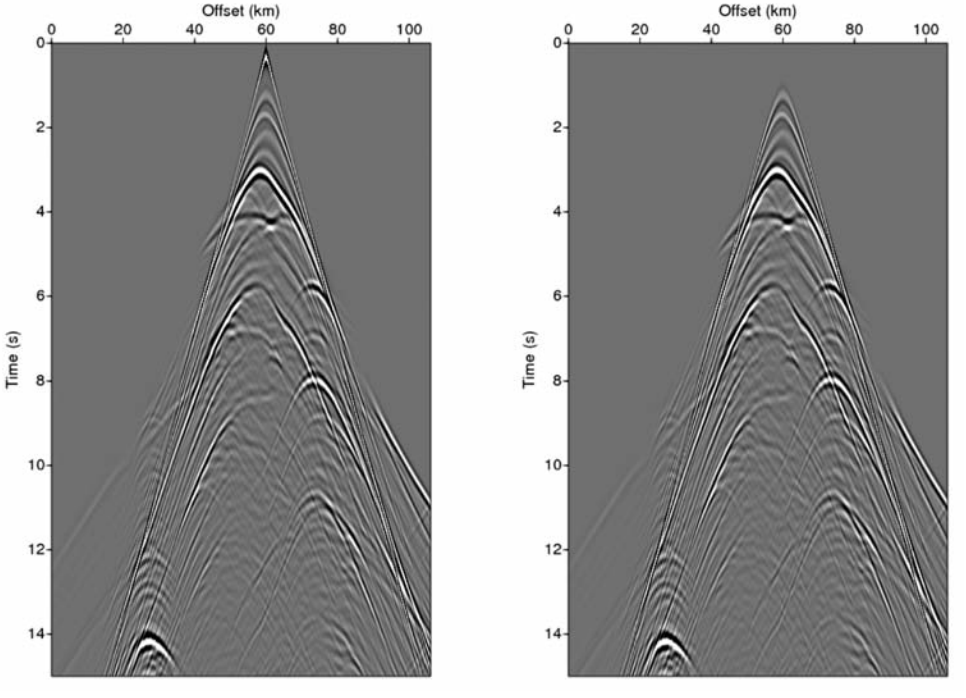

(a) (b)

Fig. 9. (a) The modeling data obtained by the second time domain finite-difference method with fourth-order spatial precision. (b) The muted data of (a).

To obtain a more definite image, we put padding layers on left and right boundaries. We then performed fourth-order time-domain finite-difference modeling in the time domain. Fig. 9(a) shows the modeling result for a 15-second time length. Fig. 9(b) shows the direct-arrival-muted data which is used to implement the DARM. The time-domain data is transformed in Laplace domain to obtain the Laplace-domain wavefield.

Fig. 10(a) shows the initial-velocity model for the waveform inversion, which increases linearly from 1.5 to 5.0 km/s.

Fig. 10(b) shows the velocity result from the conventional Laplace waveform inversion. We can observe the three salt structures in accurate positions. The thin and deep stem of the left salt dome is not definitely seen. It is difficult to obtain a thin and deep structure using Laplace waveform inversion because the wavefield from the late time signal becomes very small when taking the Laplace transform, so in the inversion its residual becomes very small.

Fig. 10(c) shows the result from the DARM. There are few differences with the conventional inversion result. To compare the inverted velocities with the true velocity, we choose two vertical velocity profiles at distances of 25 km and 38 km from the left model boundary.

Fig. 11(a) shows the vertical velocity graphs at 25 km distance. The true velocity of the salt dome is 4.5 km/s, but the inverted velocity reached 5 km/s. When performing inversion, it is necessary to control the velocity constraints cautiously. In deep regions, the DARM shows a more appropriate velocity. Fig. 11(b) shows the vertical velocity graphs at 38 km distance. The salt velocity is overestimated in the inversion; however, the inverted velocity distribution corresponds to the true velocity from the viewpoint of the long-wavelength model.

Fig. 12 shows the source wavelet (solid line), the result from the conventional source estimation using the full wavefield (diamond symbol), and the result from the new algorithm using the direct-arrival-muted wavefield (triangle symbol). In this source estimation, corresponding initial guess is 1.0 for all Laplace damping constants. The source estimation using the direct-arrival-muted wave corresponds to the true source.

Inversion of field data (Gulf of Mexico)

To perform waveform inversion in the Laplace domain, the noises in early time must be eliminated. To eliminate the noises, we normally mute the data before the direct-wave arrival time. In the case of deep-water data, a complex

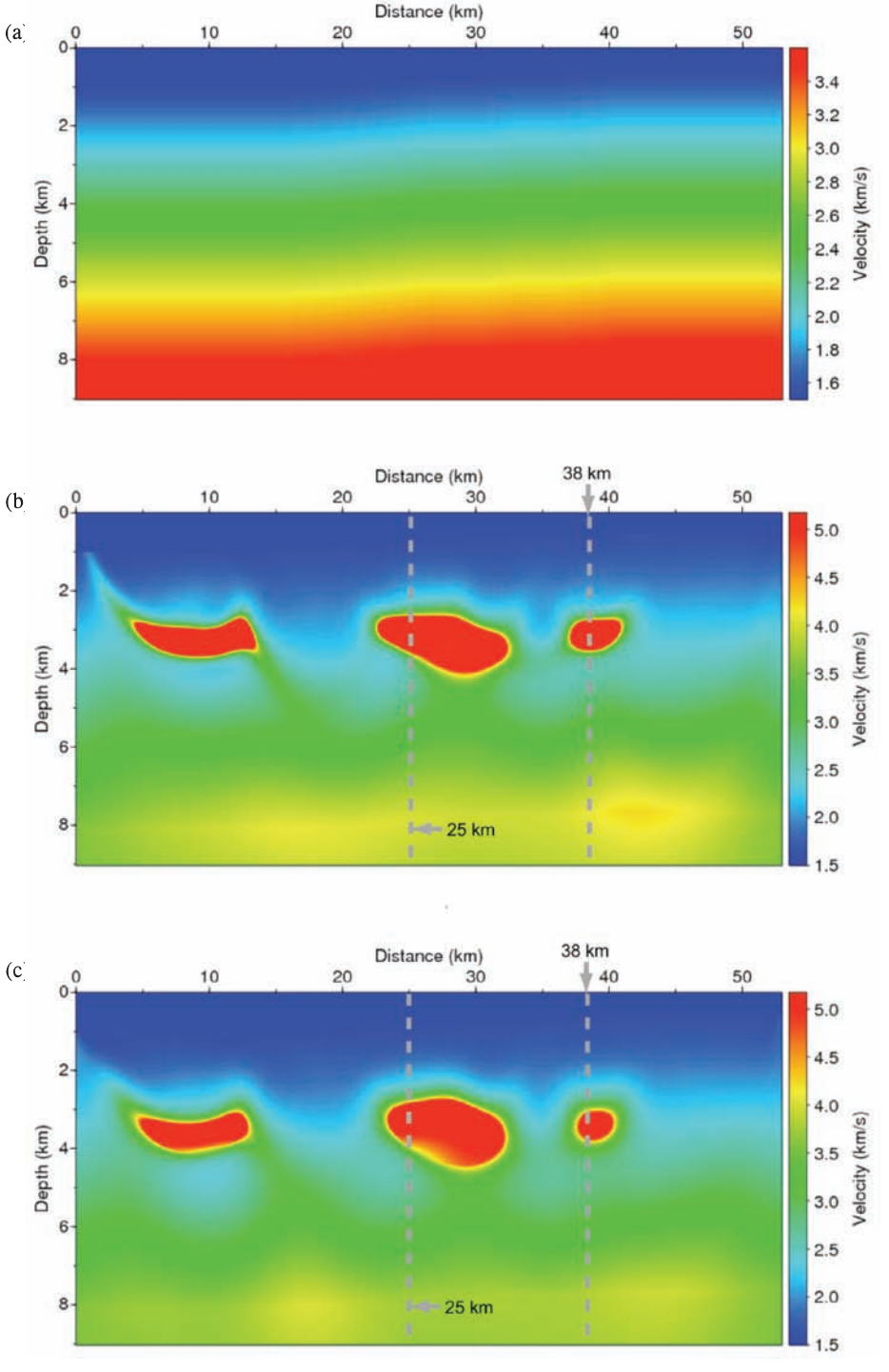

Fig. 10. (a) The initial-velocity model for the inversion test. (b) The result from a conventional

waveform inversion in the Laplace domain. (c) The result from the DARM in the Laplace domain.

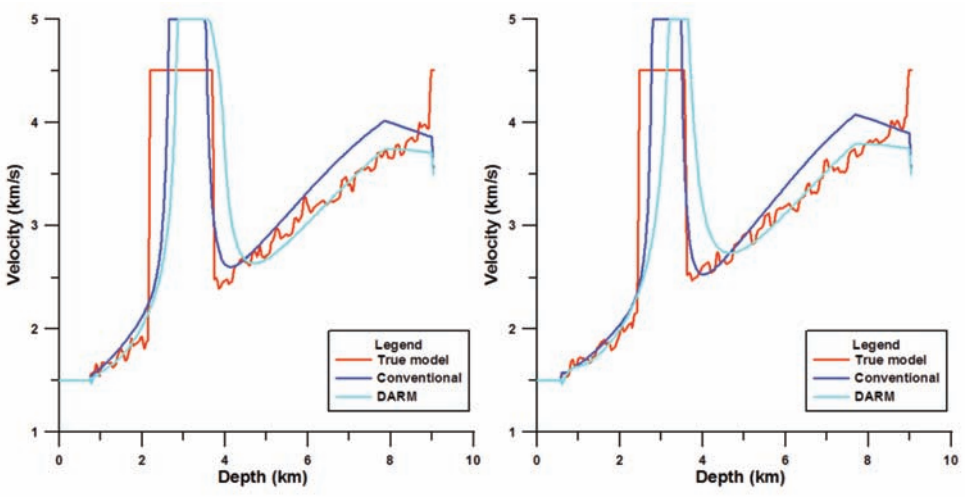

Fig. 11. Velocity profiles: (a) at 25 km distance; (b) at 38 km distance.

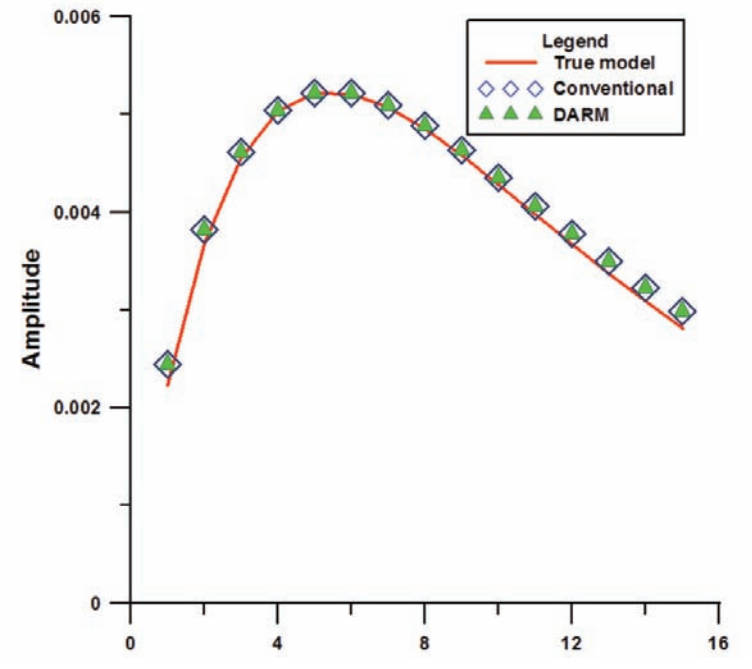

Fig. 12. Solid line, the Laplace-transformed source wavelet for the first derivative of the Gaussian wavelet from the time-domain modeling; diamonds, source wavelet estimated by the conventional

waveform inversion in the Laplace domain; triangles, source wavelet estimated by DARM in the Laplace domain.

decision was presented in muting the noise because the direct-arrival wave in long offset has a very small signal. Most first-reflection waves are greater than ambient noise. If we would not use the direct wave, it was more efficient to mute the whole signal above the first reflection from the bottom.

To verify the DARM in the Laplace waveform inversion, we tested the DARM for inverting data acquired from the Gulf of Mexico. These data has a 2-km average water depth and a 16-km distance. Fig. 13 shows the common shot gathers of (a) the original data, (b) the noise-muted data above the direct wave, and (c) the noise-muted data that does not have the direct-arrival wave. The distance between the shot and the first receiver group is 40 m, and the gap between the receiver groups is 25 m. The refraction wave is also observable, due to the wide offset spread.

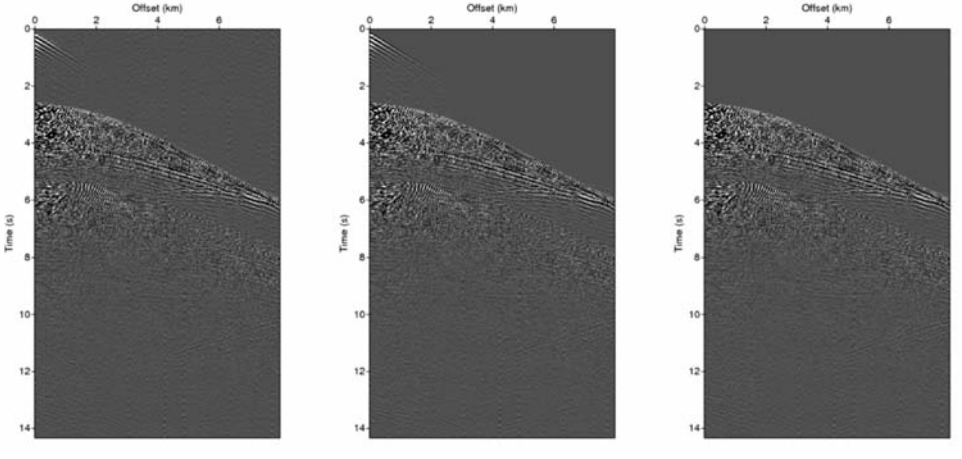

(a) (b) (c)

Fig. 13. (a) Deep-water field data from the Gulf of Mexico. (b) To implement the Laplace waveform inversion, the noise above a distinguishable direct arrival wave was muted. (c) The noise and direct arrival wave were both muted.

Fig. 14 shows the time-migration section where rms velocity picking, frequency filtering, and so on is applied. The data is known to include a salt

formation at a horizontal distance of 17-21 km. The bottom lies at 2.5-3 s. In the field test, true velocity structure is known, so this time-migration section can be useful for determining the validity of the inversion result.

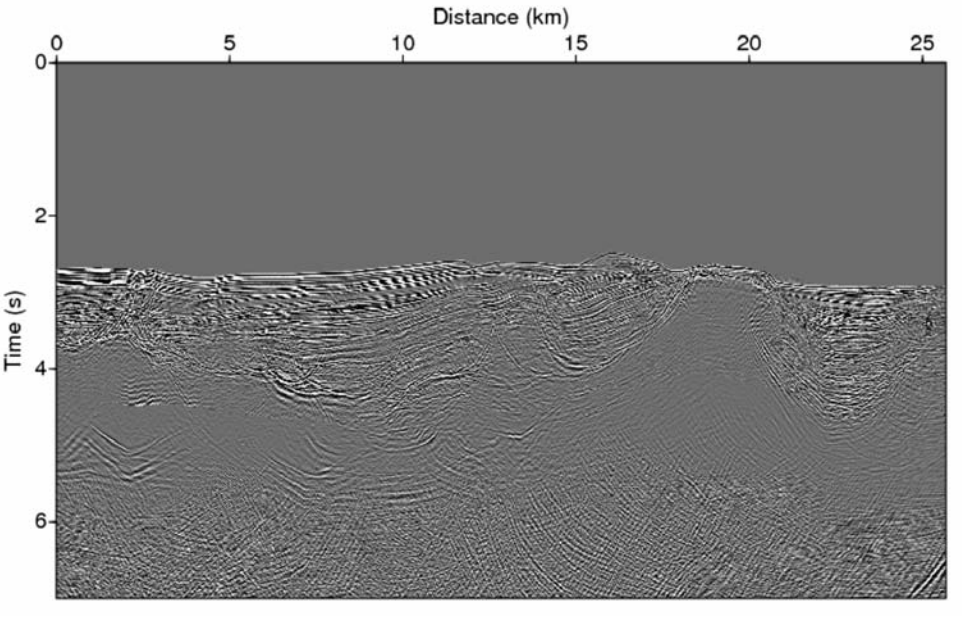

Fig. 14. Time-migration section implemented with rms velocity picking for processing field data from the Gulf of Mexico.

In this inversion test, we used a 1240 × 323 FEM mesh and the number of applied Laplace damping constants was 10, ranging from 1.0 to 10.0 in increments of 1.0. We used double-precision variables in forward and backward modeling on a 64-bit parallel Unix machine.

Fig. 15(a) shows the result from the conventional Laplace waveform inversion applying conventional muting as in Fig. 13(b). In this case, the salt region extended about 5 km along the horizontal direction and about 3 km in the vertical direction. With respect to size, the salt area was overestimated. Additionally, an abnormal high-velocity event appeared near the left boundary.

Fig. 15(b) shows the result from the DARM. The inverted salt and background velocity was more accurate than the conventional waveform inversion. For the deep-water field data, the DARM was more suitable than conventional waveform inversion in the Laplace domain.

Fig. 16 shows the transformed field data and generated forward data after finishing the conventional Laplace waveform inversion. In these plots, the vertical axis has a logarithmic scale. Especially at the position where there is a boundary indicating the direct-arrival wave, there was a large mismatch between

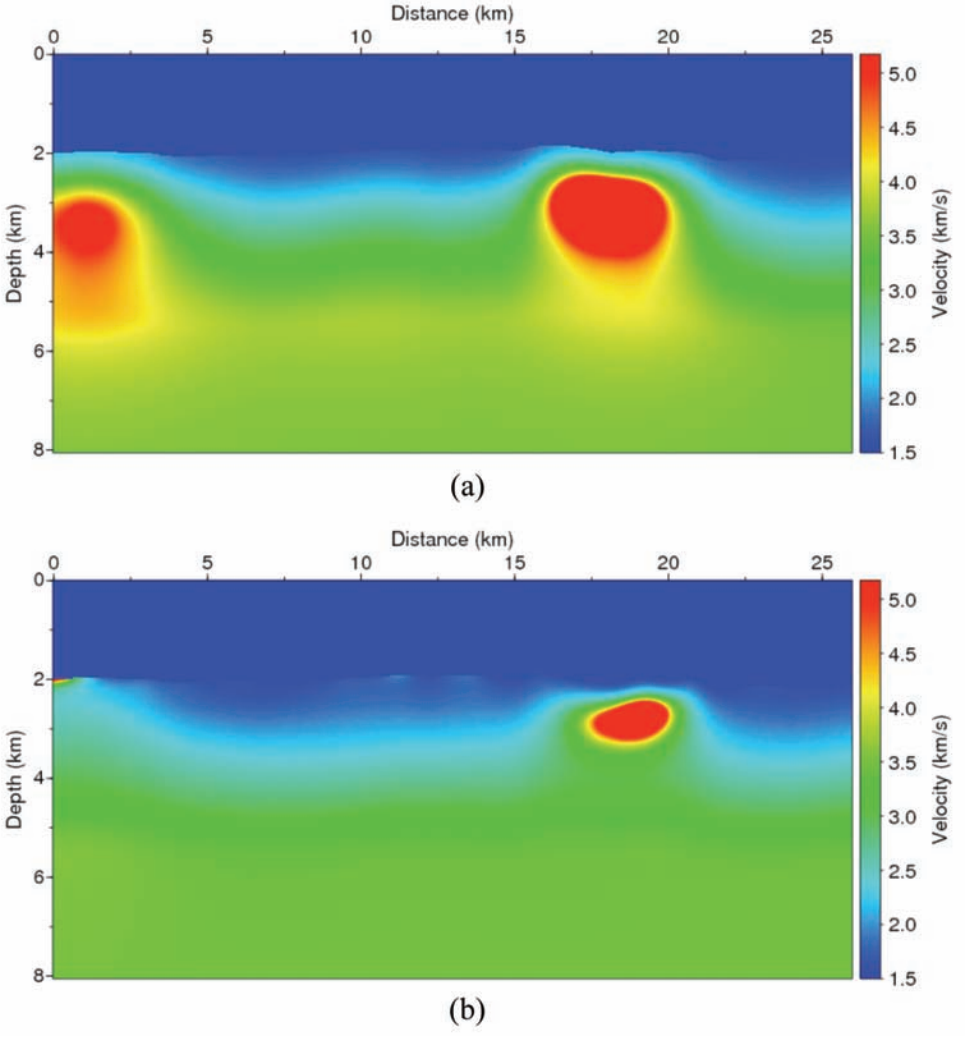

Fig. 15. (a) The inversion result from the conventional waveform inversion in the Laplace domain. (b) The result from the direct-arrival-removal method in the Laplace domain.

the field and forward-modeling waveforms. This discontinuity comes from the direct wave. The direct wave has the most significant amplitude when taking the Laplace transform in near offset, but in far offset, the direct wave has small

amplitude and the reflection wave and noise have larger amplitudes. This results in two types of data distribution. The discontinuity event is increased by increasing the Laplace damping constant, making stable convergence more difficult.

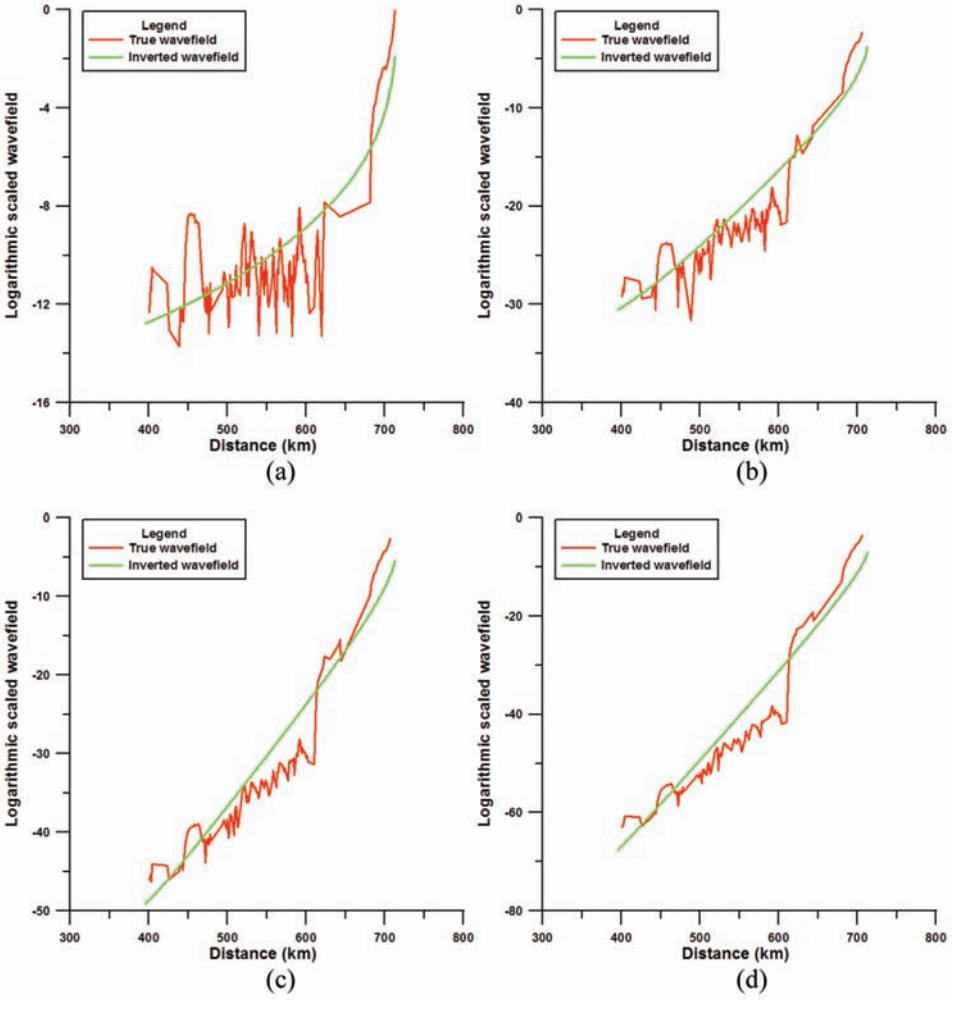

Fig. 16. Inverted wavefields compared to true wavefields after conventional waveform inversion; (a) s = 1; (b) s = 4; (c) s = 7; (d) s = 10.

Fig. 17 shows the transformed field data and generated forward data after finishing the DARM Laplace waveform inversion. There was no discontinuous position, making it easy to decrease the inversion error.

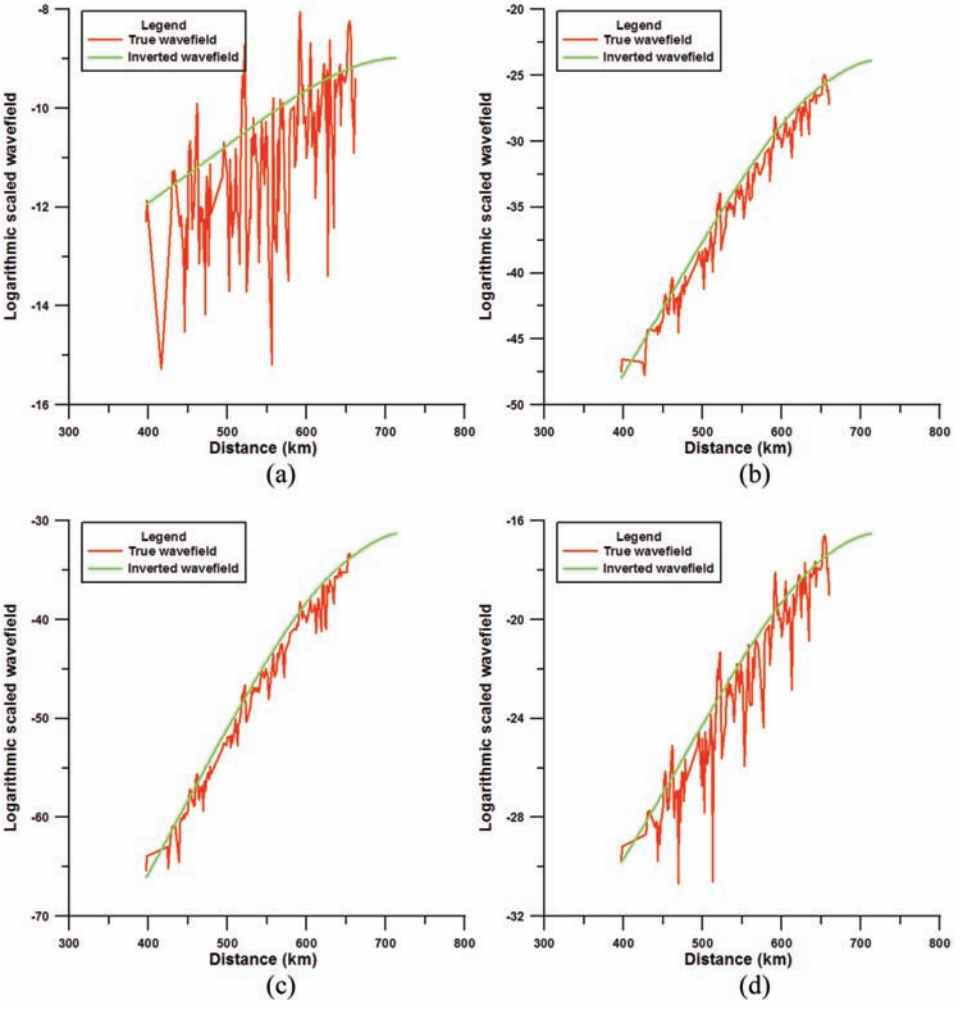

Fig. 17. Inverted wavefields compared to true wavefields after the direct-arrival-removal method; (a) s = 1; (b) s = 4; (c) s = 7; (d) s = 10.

CONCLUSIONS

Recently, deep-water seismic surveys have been implemented on the deep seafloor with depths over 1 km, such as in the Black Sea, the Atlantic Ocean off the Brazilian coast, the Gulf of Mexico, and other regions. The Laplace waveform inversion has achieved the inverted subsurface velocity structure with stability and robustness, but, in the deep-water survey, the inversion method demands modification for wavefield construction in the Laplace domain. The wavefield in the Laplace domain is sensitive to the early data. Eliminating the values in advance of the first bottom-reflection wave, including both the direct-arrival wave and the early noise, makes the wavefield more stable after taking the Laplace transform. In this study, we developed an objective function and source estimation using the DARM, and this facilitated the inversion of deep-water survey data. For a comparative study, we tested the accuracy of this DARM along with a conventional Laplace waveform inversion with a synthetic model that we then applied to deep-water field data. In the field-data test, the inversion result from the DARM was superior to the conventional Laplace waveform inversion. For obtaining the velocity structure of deep-water field data, use of the DARM would result in a more stable and efficient method in various Laplace waveform inversions.

REFERENCES

Billette, F.J. and Brandsberg-Dhal, S., 2005. The 2004 BP Velocity Benchmark. Extended Abstr., 67th EAGE Conf., Madrid: B035.

Shin, C.S. and Min, D.-J., 2006, Waveform inversion using a logarithmic wavefield. Geophysics, 7: R31-R42.

Shin, C.S., Pyun, S. and Bednar, J.B., 2007. Comparison of waveform inversion, part1: conventional wave field vs. logarithmic wavefield. Geophys. Prosp., 55: 449-464.

Shin, C.S. and Cha, Y.H., 2008. Waveform inversion in the Laplace domain. Geophys. J. Internat., 173: 922-931.

Shin, C.S. and Ha, W., 2008., A comparison between the behavior of objective functions for waveform inversion in the frequency and Laplace domains. Geophysics, 73: VE119-VE133.

Min, D.-J. and Shin, C.S., 2006. Refraction tomography using a backpropagation technique of waveform inversion. Geophysics, 71: R21-R30.

Pratt, R.G., Shin, C.S. and Hicks, G.J., 1998. Gauss-Newton and full Newton methods in frequency-space seismic-waveform inversion. Geophys. J. Internat., 133: 341-362.

Kim, Y., Cha, Y.-H., Shin, C.S., Ko, S. and Seo, Y., 2009. Improved logarithmic waveform inversion considering the power-spectrum of the wavefield. J. Seismic Explor., 18: 215-228.

Tarantola, A., 1984. Inversion of seismic reflection data in the acoustic approximation. Geophysics, 49: 1259-1266.